ELSEVIER

23 August 1996

Chemical Physics Letters 258 (1996) 523–529

CHEMICAL PHYSICS LETTERS

Photodissociation dynamics of the I_2^- anion using femtosecond photoelectron spectroscopy

B. Jefferys Greenblatt [a,b], Martin T. Zanni [a,b], Daniel M. Neumark [a,b]

[a] *Department of Chemistry, University of California, Berkeley, CA 94720, USA*
[b] *Chemical Sciences Division, Lawrence Berkeley National Laboratory, Berkeley, CA 94720, USA*

Received 20 June 1996

Abstract

The photodissociation dynamics of the I_2^- anion have been studied in real-time using femtosecond photoelectron spectroscopy. In this experiment, I_2^- is excited to a dissociative electronic state with an ultrafast pump pulse, and the photoelectron spectrum of the dissociating anion is measured by photodetachment with a second, ultrafast probe pulse. The variation of the photoelectron spectrum with delay time enables one to monitor the dissociating anion from the initial Franck–Condon region of excitation out to the asymptotic region. Dissociation occurs on a time scale of 100 fs. The results are compared with quantum mechanical simulations using previously published potential energy curves for I_2^-.

1. Introduction

The successful application of time-resolved techniques to gas phase processes occurring on a femtosecond time scale has been one of the most important developments in chemical dynamics during the last ten years [1,2]. The considerable body of work in this area has provided new insights into the photodissociation and reaction dynamics of molecules and clusters. However, nearly all gas-phase femtosecond experiments performed to date have focused on neutral species. The application of these methods to ions, particularly negative ions, is very appealing. In contrast to neutral species, most potential energy surfaces involving negative ions are poorly characterized. The low number densities typical of gas phase negative ion experiments make it difficult to study the spectroscopy and dynamics of these species using frequency-resolved techniques, such as absorption spectroscopy, laser-induced fluorescence, or multi-photon ionization, that are applied almost routinely to neutral species. Hence, the photodissociation and reaction dynamics of negative ions represent fertile ground for time-resolved experiments. The desirability and feasibility of performing time-resolved experiments on mass-selected anions has been demonstrated in the pioneering work by Lineberger and co-workers [3–6] on dissociation and caging dynamics in $I_2^-(CO_2)_n$ clusters.

These cluster studies provide the motivation for the work described here, in which the photodissociation dynamics I_2^- are investigated using femtosecond photoelectron spectroscopy (FPES). This is a relatively new technique which, along with the related technique of femtosecond zero electron kinetic energy spectroscopy [7,8], has recently been applied to excited state dynamics in neutral molecules [9,10]. The results here represent the first application of FPES to negative ions. FPES is a pump-and-probe experiment involving two femtosecond pulses. In our

PII S0009-2614(96)00766-X

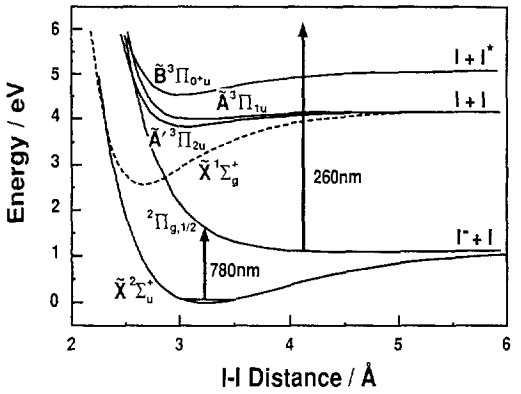

Fig. 1. Potential energy curves for relevant electronic states of I_2^- and I_2 taken from Refs. [11,19–21].

experiment, the first pulse ($h\nu_1$) electronically excites the I_2^- to a repulsive state, and the second ($h\nu_2$) photodetaches the dissociating molecule to form a photoelectron and either two I atoms or an excited I_2 molecule. The overall process is given by

$$I_2^- \xrightarrow[h\nu_1]{} I_2^{-*} \xrightarrow[\Delta t]{} I^-...I \xrightarrow[h\nu_2]{} I_2 + e^-, I + I + e^-. \quad (1)$$

By measuring the photoelectron kinetic energy spectrum as a function of delay time Δt, one can monitor the dissociation dynamics of the electronically excited I_2^- all the way from the Franck–Condon region to the dissociation asymptote.

The I_2^- anion was chosen for these first studies because of its experimental accessibility, and because it is a fundamentally important anion in gas phase and solution phase chemistry. Chen and Wentworth [11] constructed a set of potential energy curves for the ground and excited states of I_2^- based on Raman spectroscopy in a rare gas matrix, electronic spectroscopy in a crystal, and gas phase dissociative attachment experiments. However, questions remain concerning the accuracy of these curves. For example, the I_2^- electronic spectrum clearly depends on the environment of the ion; the bands in rare gas matrices are shifted by 0.16–0.27 eV to the blue of the bands in a crystalline environment [12–14], and one expects the gas phase spectrum to differ from either condensed phase spectrum. Recent dissociative attachment results [15] also suggest that the I_2^- potential energy curves in Ref. [11] need to be modified. These curves have been used to simulate time-resolved dynamics of I_2^- in clusters [16] and in various solvents [17,18], so it is important that they be as accurate as possible. The results presented here provide an independent test of the available potential energy curves for I_2^-.

Fig. 1 shows the potential energy curves involved in our experiments. I_2^- is excited from its ground $\tilde{X}^2\Sigma_u^+$ state to the low-lying $^2\Pi_{g,1/2}$ excited state by the pump pulse with photon energy $h\nu_1$. The time-dependence of the resulting wavepacket is monitored by measuring its photoelectron spectrum. The photodetaching probe pulse, $h\nu_2$, has sufficient energy to access the $\tilde{X}^1\Sigma_g^+$, $\tilde{A}'^3\Pi_{2u}$, $\tilde{A}^3\Pi_{1u}$, and $\tilde{B}^3\Pi_{0^+u}$ states of I_2. At short delay times, photodetachment will access bound vibrational levels of these I_2 states, but at longer times, when dissociation to $I^- + I$ is complete, one is essentially photodetaching a free I^- ion. Hence, the photoelectron spectrum of the dissociating wavepacket should change substantially with delay time. Since the I_2 states are well characterized [19–21], the time-resolved photoelectron spectra should serve as a probe of the anion states, as desired.

2. Experimental

The experiment consists of two major components: a negative ion photoelectron spectrometer with a 'magnetic bottle' electron detector, and a high (1 kHz) repetition rate laser capable of generating sub-

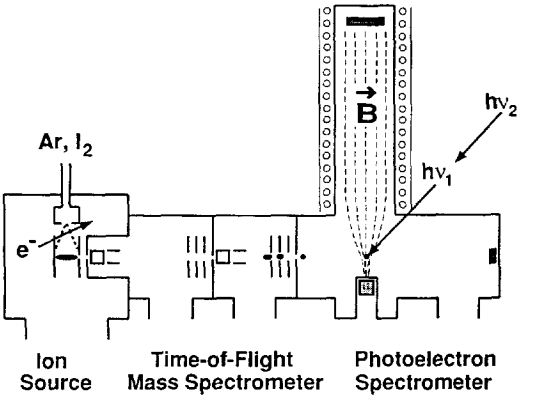

Fig. 2. Schematic of apparatus, showing ion source region, time-of-flight mass spectrometer, and 'magnetic bottle' photoelectron time-of-flight spectrometer.

100 fs pulses. The photoelectron spectrometer is shown in Fig. 2. It shares several features with spectrometers currently in operation in our laboratory [22] as well as others [23–25], but is optimized in design so as to be compatible with the laser repetition rate and pulse energy.

I_2^- anions are generated in a continuous free jet ion source by passing Ar carrier gas at 20 psig over I_2, expanding the resulting mixture through a 100 μm orifice into the source chamber, and crossing the resulting molecular beam just downstream of the orifice with 1 keV electrons from an electron gun. The source chamber is pumped by two Varian VHS-10 diffusion pumps for a total pumping speed of 8800 l/sec. Ions are extracted from the beam and injected into a Wiley–McLaren time-of-flight mass spectrometer [26] by applying pulsed extraction and acceleration fields perpendicular to the molecular beam axis; the final ion beam energy is about 1200 eV. Once the ions are accelerated, they pass through two differentially pumped regions en route to the laser interaction region. The first differential region is pumped by a Varian VHS-6 diffusion pump. The second differential region and laser interaction region are pumped by Varian V250 turbomolecular pumps, and the base pressure in the latter region is 2×10^{-9} Torr. An in-line microchannel plate detector is used to obtain the time-of-flight mass spectrum of the ion beam.

The ion beam is crossed by the laser pulses 55 cm upstream of the ion detector. A large fraction (> 50%) of the resulting photoelectrons is collected using a magnetic bottle time-of-flight photoelectron spectrometer based on the design of Cheshnovsky et al. [24], although we use a strong (0.8 tesla) permanent magnet rather than an electromagnet to generate the inhomogeneous magnetic field. The electrons are collected at a 75 mm diameter microchannel plate detector 1.4 m from the interaction region, and the arrival time distribution is recorded after each laser shot with a Stanford Research Systems SR430 multichannel scalar. The energy resolution of the spectrometer is currently 150–300 meV, depending on the electron kinetic energy; this will be improved in the near future by pulsed deceleration of the ion beam [24,25].

The pump and probe laser pulses are generated from a commercial femtosecond laser system. A Coherent Innova-90 Ar^+ laser pumps a Clark-MXR NJA-5 Ti:sapphire oscillator. Selected pulses are amplified using a Clark-MXR regenerative amplifier system that includes a pulse stretcher, a Ti:sapphire regenerative amplifier pumped by a Nd:YAG laser running at a repetition rate of 1 kHz, and a pulse compressor. At 780 nm, the pump pulse wavelength, the pulse width and energy are 80 fs and 1 mJ, respectively. About 70% of this beam is directed into a frequency tripling unit (CSK Optronics 8315A), resulting in a probe pulse at 260 nm with width and energy of 110 fs and 20 μJ, respectively. (The pulse width of the probe pulse is measured by cross-correlation with the pump pulse using a KDP crystal for frequency differencing.) The remainder of the 780 nm pulse passes through a variable delay line and is then collinearly recombined with the probe pulse prior to entering the vacuum chamber.

The UV probe pulse spreads when it passes through the vacuum chamber window, and this window also affects the delay between the pump and probe pulses. Two-color above threshold detachment (ATD) of I^- is used to characterize the laser pulses inside the vacuum chamber [27]. The probe pulse alone produces the characteristic photoelectron spectrum of I^- (see below). When the pump and probe pulses temporally overlap, additional peaks are observed that correspond to shifting the I^- spectrum by 1.6 eV towards higher electron kinetic energy; this is the photon energy of the pump pulse. From the intensity of this two-color signal as a function of pump–probe delay, we determine the zero-delay time and the cross-correlation of the pump and probe pulses inside the vacuum chamber. This yields a pulse width of 140 fs for the probe pulse.

The combination of high laser repetition rate and high electron collection efficiency results in rapid data collection. In the data set presented below, only 50 s of data collection are required at each time delay. The spectra are not background-free because one probe photon can photodetach ground state I_2^-. At each time delay, background subtraction is accomplished by collecting 50% of the data (i.e. for 25 s) at long negative delays (−2 ps), where the probe pulse fires well before the pump pulse. This background is suitably scaled and subtracted from the raw spectra to yield the spectra in the following section.

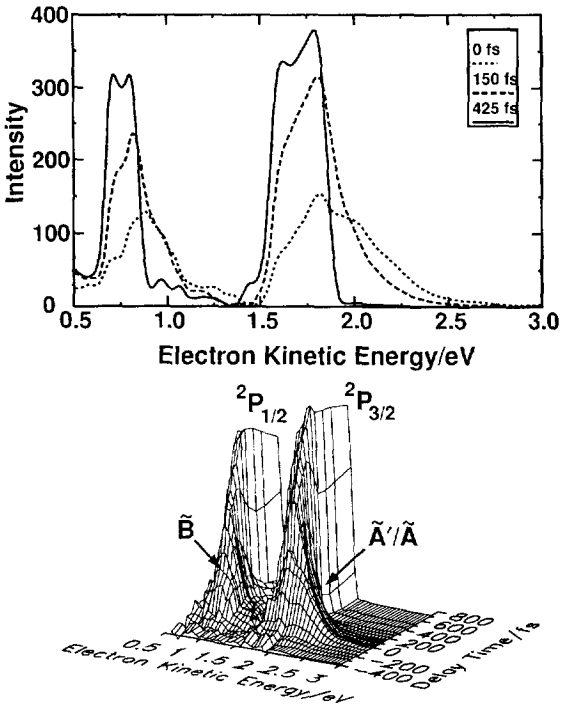

Fig. 3. Experimental femtosecond photoelectron spectra of I_2^-. Upper panel: spectra at three delay times. Lower panel: spectra at 21 delay times ranging from −400 to 725 fs. Assignments of various energy ranges are indicated. The dark lines shows the delay time at which the maximum intensity of transient signal occurs for each electron kinetic energy.

3. Results and analysis

Experimental results are shown in Fig. 3. In the top half of Fig. 3, three photoelectron spectra are superimposed, at $\Delta t = 0$, 150, and 425 fs. The spectrum at the longest delay time, $\Delta t = 425$ fs, is essentially the I^- photoelectron spectrum; the two peaks centered at 0.75 and 1.7 eV represent transitions to the $I(^2P_{3/2})$ and $I^*(^2P_{1/2})$ states, respectively. A comparison with the two spectra at shorter delay times shows that the intensities of these atomic transitions increase monotonically with Δt. In addition, there is a transient signal on the high electron kinetic energy side of each atomic transition that is of comparable intensity in the spectra at $\Delta t = 0$ and 150 fs but has decayed to zero by $\Delta t = 425$ fs. A comparison of the spectra at $\Delta t = 0$ and 150 fs shows that the transient signal is shifted towards the atomic transitions at the longer delay time.

The full data set of 21 photoelectron spectra is shown as a three-dimensional surface plot in the bottom half of Fig. 3. This plot emphasizes the temporal structure of the signal at each electron kinetic energy, and shows that depending on the electron kinetic energy, the signal is either monotonically increasing or transient with a full width at half-maximum (FWHM) of about 200 fs. The value of Δt at which the transient signal reaches a maximum depends on the electron kinetic energy, as indicated by the dark lines in Fig. 3. As the electron kinetic energy decreases (i.e. moves towards the atomic transition), the maximum occurs at longer values of Δt.

The monotonically increasing I^- signal clearly comes from fully dissociated I_2^-. The transient signal can be assigned with reference to the potential energy curves in Fig. 1. At 260 nm, the $\tilde{X}\,^1\Sigma_g^+$, $\tilde{A}'\,^3\Pi_{2u}$, $\tilde{A}\,^3\Pi_{1u}$, and $\tilde{B}\,^3\Pi_{0^+u}$ states of I_2 should be energetically accessible by photodetachment from the excited I_2^- $^2\Pi_{g,1/2}$ state over the full range of internuclear distances probed in the experiment. However, the $\tilde{X}\,^1\Sigma_g^+$ state of I_2 cannot be reached by a one-electron photodetachment transition from the $^2\Pi_{g,1/2}$ state of I_2^-; the valence molecular orbital configurations for these states are $\sigma_g^2\,\pi_u^4\,\pi_g^4$ and $\sigma_g^2\,\pi_u^4\,\pi_g^3\,\sigma_u^2$, respectively. Transitions from the excited anion to the $\tilde{X}\,^1\Sigma_g^+$ state should therefore be weak or non-existent, whereas the other three states are accessible by one-electron photodetachment transitions. Fig. 1 shows that the excited anion and neutral potential energy curves are closer at short internuclear distances than in the asymptotic region. We therefore assign the transient signal on the high kinetic energy side of the $I^- \rightarrow I(^2P_{3/2})$ and $I^- \rightarrow I^*(^2P_{1/2})$ peaks to transitions from the dissociating anion to the $\tilde{A}'\,^3\Pi_{2u}/\tilde{A}\,^3\Pi_{1u}$ states and the $\tilde{B}\,^3\Pi_{0^-u}$ state, respectively; these assignments are indicated in Fig. 3.

In order to interpret the spectra in more detail, quantum mechanical simulations of the time-resolved photoelectron spectra have been performed, using a wavepacket propagation scheme developed by Kosloff [28]. Wavefunctions $|\psi_n(t)\rangle$ with $n = 1$, 2 or 3, are represented on a spatial grid for each of three potential energy curves: $1 = I_2^-$ $(\tilde{X}\,^2\Sigma_u^+)$; $2 = I_2^-$ $(^2\Pi_{g,1/2})$; $3 = I_2$ $(\tilde{A}'\,^3\Pi_{2u}$, $\tilde{A}\,^3\Pi_{1u}$, or $\tilde{B}\,^3\Pi_{0^+u})$. Morse functions [11,19–21] were used for all states.

The simulations are carried out in two steps. The wavepacket for the dissociating anion, $|\psi_2(t)\rangle$, is found by numerically integrating the time-dependent Schrödinger equation

$$i\hbar\frac{d}{dt}\begin{pmatrix}|\psi_1(t)\rangle\\|\psi_2(r)\rangle\end{pmatrix}=\begin{pmatrix}H_1 & -\mu_{12}E_{12}^*(t)\\-\mu_{12}E_{12}(t) & H_2\end{pmatrix}\times\begin{pmatrix}|\psi_1(t)\rangle\\|\psi_2(t)\rangle\end{pmatrix}. \quad (2)$$

Here H_n is the nuclear Hamiltonian for state n, $E_{12}(t)=E_{12}\,\mathrm{sech}(t/T_{12})\exp(-i\omega_{12}t)$ is the time-dependent pump laser field (E_{12} is the maximum field intensity; T_{12} the pulse width; ω_{12} the carrier frequency), and μ_{12} is the transition dipole moment between states 1 and 2, assumed to be constant for all internuclear distances.

First order perturbation theory is then used to calculate $|\psi_3(t;\ \epsilon,\ \Delta t)\rangle$, the neutral vibrational wavefunction corresponding to electron kinetic energy ϵ [29]. This is given by

$$|\psi_3(t;\epsilon,\Delta t)\rangle=\frac{i\mu_{23}}{\hbar}\int_{-\infty}^{t}dt'\,e^{-i(H_3+\epsilon)(t-t')/\hbar}E_{23}\times(t'-\Delta t)|\psi_2(t')\rangle,$$

where Δt is the time delay between pump and probe pulses, H_3 is the nuclear Hamiltonian for state 3, ϵ is the electron kinetic energy, and $E_{23}(t-\Delta t)$ is the probe laser field, with the same assumed functional form as for $E_{12}(t)$. The transition dipole moment μ_{23} is again assumed to be constant for all distances. The time-dependent photoelectron intensity is then obtained by calculating the norm of $|\psi_3\rangle$ in the long-time limit [29,30]:

$$P(\epsilon,\Delta t)=\lim_{t\to\infty}\langle\psi_3(t;\epsilon,\Delta t)|\psi_3(t;\epsilon,\Delta t)\rangle=\frac{|\mu_{23}|^2}{\hbar^2}\left|\int_{-\infty}^{\infty}dt'\,e^{i\epsilon t'/\hbar}\times\left[E_{23}(t'-\Delta t)e^{iH_3t'/\hbar}|\psi_2(t')\rangle\right]\right|^2. \quad (4)$$

Note that the bracketed expression in the integrand is the argument of a Fourier transform. Thus, once the set of wavefunctions $|\chi(t')\rangle=e^{iH_3t'/\hbar}|\psi_2(t')\rangle$ is determined, the entire photoelectron spectrum is readily calculated. In addition, since $E_{23}(t'-\Delta t)$ is a scalar multiplier, it can be applied independently of $|\chi(t')\rangle$, allowing calculation of the spectrum for arbitrary Δt or probe pulse shape without re-determining $|\psi_2(t')\rangle$.

Raw spectra were convoluted with the instrument resolution function for an isotropic electron angular distribution, assuming electrons are collected over 4π steradians in our experiment:

$$p(E,\epsilon)=\sqrt{1-\frac{M}{4m_eU\epsilon}\left(E-\epsilon-\frac{m_eU}{M}\right)^2}. \quad (5)$$

Here M = ion mass, m_e = electron mass, U = ion beam energy, ϵ = electron kinetic energy (center-of-mass frame) and E = electron kinetic energy (lab frame). Using $M=254$ amu and $U=1200$ eV gives an energy resolution of 0.20 eV for 1 eV electrons, in good agreement with experiment.

The spectra arising from transitions to the three neutral states of I_2 are calculated separately, then summed using the following weighting criterion: μ_{23} is assumed equal for transitions to the $\tilde{A}'^3\Pi_{2u}$ and $\tilde{A}^3\Pi_{1u}$ states, and μ_{23} for the transition to the $\tilde{B}^3\Pi_{0^+u}$ state is adjusted so that the ratio of $I^*(^2P_{1/2})$ to $I(^2P_{3/2})$ intensities (at large delay time) reproduces the experimental value of 0.9.

The simulated spectra are shown in Fig. 4. Overall, the experimental and simulated spectra are in reasonable agreement. The transient signal appears over the same energy range in both the experimental and simulated spectra, indicating that our assignment

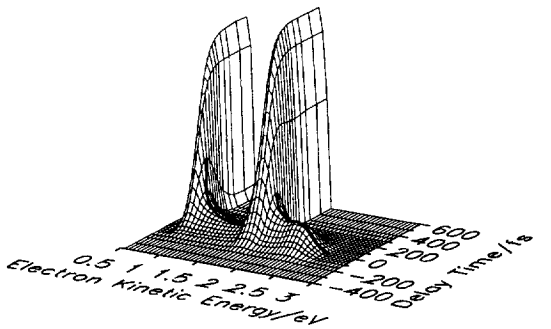

Fig. 4. Simulated femtosecond photoelectron spectra of I_2^- using Eq. (4) in text. Delay times range from −400 to 600 fs. The dark lines show the delay time at which the maximum intensity of transient signal occurs for each electron kinetic energy.

of the transient features discussed above is correct. However, there clearly are differences between the two spectra, and these are discussed in the next section.

4. Discussion

From the experimental spectra alone, one can obtain an approximate time scale for dissociation of excited I_2^- from the rise time of the signal corresponding to the product atomic transitions. This is plotted in Fig. 5 for electron kinetic energies of 1.65 and 0.75 eV, corresponding to the $I^- \rightarrow I(^2P_{3/2})$ and $I^- \rightarrow I(^2P_{1/2})$ transitions, respectively. In both cases, the electron signal reaches 50% of its maximum value by $\Delta t = 100$ fs. A more detailed picture of the dynamics comes from the temporal profiles at constant electron kinetic energy. As the electron kinetic energy decreases from the onset of the $\tilde{A}'/\tilde{A}$ transient at 2.6 eV to the start of the $I^- \rightarrow I(^2P_{3/2})$ transition at 1.9 eV, the maximum in the temporal profile (dark line, Fig. 3) increases from $\Delta t = 10$ to $\Delta t = 110$ fs. A similar shift is seen for the $\tilde{B}$ transient. This shift essentially tracks the dissociating wavepacket from the initial Franck–Condon region of excitation at short times, where the vertical detachment energy from the anion $^2\Pi_{g,1/2}$ state is smaller (see Fig. 1), to the asymptotic region at longer times where the vertical detachment energy is larger.

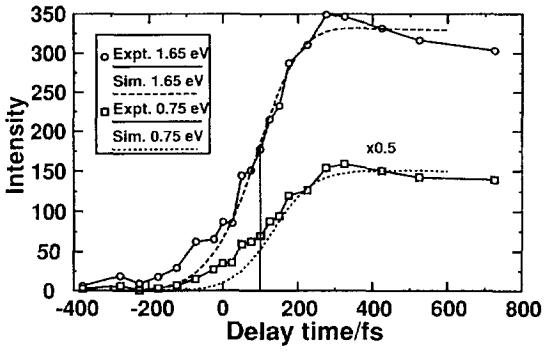

Fig. 5. Appearance of signal versus delay time at electron kinetic energies of 1.65 and 0.75 eV, corresponding to I^- product. Solid lines: experimental spectra. Dashed lines: simulated spectra. Vertical line indicates $\Delta t = 100$ fs.

We next compare the experimental and simulated spectra. The transient signals are noticeably less intense in the simulated spectra, and there is a broad peak centered at 2.5 eV and $\Delta t = 0$ fs in the simulated spectra that is not apparent in the experimental spectra. However, the overall time scales in the simulated spectra are similar to those in the experiment. Fig. 5 shows that the 50% level of the simulated signal at 1.65 eV occurs at 100 fs, with a slightly longer rise time (120 fs) at 0.75 eV. From Fig. 4, the maxima in the temporal profiles shift by 100 fs in the energy range of the two transients.

The lower intensity in the simulated spectra may simply result from our assumption that the transition dipole for photodetachment, μ_{23}, is constant in Eq. (3); this discrepancy would be resolved if μ_{23} were larger for small internuclear distances, before dissociation is complete. On the other hand, it appears that the potential energy curves used in the simulations reproduce the main features of the experimental dynamics reasonably well. A new set of I_2^- potential energy curves has just been published [31], and it will be of interest to simulate the spectra using these new curves and compare the results to experiment.

5. Summary

This Letter represents the first application of femtosecond photoelectron spectroscopy to negative ions, specifically the photodissociation dynamics of I_2^-. This method offers considerable promise for performing time-resolved studies of molecular and cluster anions. The general advantage afforded by FPES is that the probe pulse need not be tunable; the photoelectron spectrum maps out the dissociating anion state onto all neutral states that are energetically accessible at the photon energy of the probe laser. In the case of I_2^-, the wavefunction for the dissociating anion is simultaneously mapped onto the $\tilde{A}'\,^3\Pi_{2u}$, $\tilde{A}\,^3\Pi_{1u}$, and $\tilde{B}\,^3\Pi_{0^+u}$ states of I_2. Moreover, since electron binding energies in negative ions are relatively low, only one photon is typically required to photodetach the dissociating ion anywhere along the reaction coordinate. One can therefore analyze the spectra relatively easily, in contrast to analogous experiments on neutrals where multiple photon absorption is typically required for ionization.

Acknowledgements

This research is supported by the National Science Foundation under Grant No. CHE-9404735. Support from the Defense University Research Instrumentation Program and Air Force Office of Scientific Research under Grant No. F49620-95-1-0078 is also gratefully acknowledged. The authors thank Professor Yonqin Chen for many invaluable discussions.

References

[1] A.H. Zewail, J. Phys. Chem. 97 (1993) 12427.
[2] J.C. Polanyi and A.H. Zewail, Acc. Chem. Res. 28 (1995) 119.
[3] D. Ray, N.E. Levinger, J.M. Papanikolas and W.C. Lineberger, J. Chem. Phys. 91 (1989) 6533.
[4] J.M. Papanikolas, J.R. Gord, N.E. Levinger, D. Ray, V. Vorsa and W.C. Lineberger, J. Phys. Chem. 95 (1991) 8028.
[5] J.M. Papanikolas, V. Vorsa, M.E. Nadal, P.J. Campagnola, J.R. Gord and W.C. Lineberger, J. Chem. Phys. 97 (1992) 7002.
[6] J.M. Papanikolas, V. Vorsa, M.E. Nadal, P.J. Campagnola, H.K. Buchenau and W.C. Lineberger, J. Chem. Phys. 99 (1993) 8733.
[7] T. Baumert, R. Thalweiser and G. Gerber, Chem. Phys. Lett. 209 (1993) 29.
[8] I. Fischer, D.M. Villeneuve, M.J.J. Vrakking and A. Stolow, J. Chem. Phys. 102 (1995) 5566.
[9] B. Kim, C.P. Schick and P.M. Weber, J. Chem. Phys. 103 (1995) 6903.
[10] D.R. Cyr and C.C. Hayden, J. Chem. Phys. 104 (1996) 771.
[11] E.C.M. Chen and W.E. Wentworth, J. Phys. Chem. 89 (1985) 4099.
[12] H.N. Hersh, J. Chem. Phys. 31 (1959) 909.
[13] C.J. Delbecq, W. Hayes and P.H. Yuster, Phys. Rev. 121 (1961) 1043.
[14] L. Andrews, J. Am. Chem. Soc. 98 (1976) 2152.
[15] R. Azria, R. Abouaf and D. Teillet-Billy, J. Phys. B 21 (1988) L213.
[16] J.M. Papanikolas, P.E. Maslen and R. Parson, J. Chem. Phys. 102 (1995) 2452.
[17] A.E. Johnson, N.E. Levinger and P.F. Barbara, J. Phys. Chem. 96 (1992) 7841.
[18] P.K. Walhout, J.C. Alfano, K.A.M. Thakur and P.F. Barbara, J. Phys. Chem. 99 (1995) 7568.
[19] J.I. Steinfeld, R.N. Zare, L. Jones, M. Lesk and W. Klemperer, J. Chem. Phys. 42 (1965) 25.
[20] X. Zheng, S. Fei, M.C. Heaven and J. Tellinghuisen, J. Molec. Spectrosc. 149 (1991) 399.
[21] X. Zheng, S. Fei, M.C. Heaven and J. Tellinghuisen, J. Chem. Phys. 96 (1992) 4877.
[22] R.B. Metz, A. Weaver, S.E. Bradforth, T.N. Kitsopoulos and D.M. Neumark, J. Phys. Chem. 94 (1990) 1377.
[23] L.A. Posey, M.J. DeLuca and M.A. Johnson, Chem. Phys. Lett. 131 (1986) 170.
[24] O. Cheshnovsky, S.H. Yang, C.L. Pettiette, M.J. Craycraft and R.E. Smalley, Rev. Sci. Instrum. 58 (1987) 2131.
[25] C.-Y. Cha, G. Gantefor and W. Eberhardt, Rev. Sci. Instrum. 63 (1992) 5661.
[26] W.C. Wiley and I.H. McLaren, Rev. Sci. Instrum. 26 (1955) 1150.
[27] M.D. Davidson, B. Broers, H.G. Muller and H.B. van Linden van den Heuvell, J. Phys. B 25 (1992) 3093.
[28] R. Kosloff, J. Phys. Chem. 92 (1988) 2087.
[29] C. Meier and V. Engel, Phys. Rev. Lett. 73 (1994) 3207.
[30] M. Seel and W. Domcke, J. Phys. Chem. 95 (1991) 7806.
[31] J.G. Dojahn, E.C.M. Chen and W.E. Wentworth, J. Phys. Chem. 100 (1996) 9649.